Exploration of the Kuiper Belt by High-Precision Photometric Stellar Occultations: First Results

F. Roques, A. Doressoundiram, V. Dhillon, T. Marsh, S. Bickerton, J. J. Kavelaars, M. Moncuquet, M. Auvergne, I. Belskaya, M. Chevreton, et al.

The Astronomical Journal, 132:819–822, 2006 August

EXPLORATION OF THE KUIPER BELT BY HIGH-PRECISION PHOTOMETRIC STELLAR OCCULTATIONS: FIRST RESULTS

F. Roques,[1,2] A. Doressoundiram,[1] V. Dhillon,[3] T. Marsh,[4] S. Bickerton,[5,6] J. J. Kavelaars,[5] M. Moncuquet,[1] M. Auvergne,[1] I. Belskaya,[7] M. Chevreton,[1] F. Colas,[1] A. Fernandez,[1] A. Fitzsimmons,[8] J. Lecacheux,[1] O. Mousis,[9] S. Pau,[1] N. Peixinho,[1,10] and G. P. Tozzi[11]

Received 2005 November 11; accepted 2006 May 4

ABSTRACT

We report here the first detection of hectometer-size objects by the method of serendipitous stellar occultation. This method consists of recording the diffraction shadow created when an object crosses the observer's line of sight and occults the disk of a background star. One of our detections is most consistent with an object between Saturn and Uranus. The two other diffraction patterns detected are caused by Kuiper Belt objects beyond 100 AU from the Sun and hence are the farthest known objects in the solar system. These detections show that the Kuiper Belt is much more extended than previously believed and that the outer part of the disk could be composed of smaller objects than the inner part. This gives critical clues to understanding the problem of the formation of the outer planets of the solar system.

Key words: Kuiper Belt — occultations — solar system: formation

1. INTRODUCTION

The Kuiper Belt is the remnant of the circumsolar disk where the giant planets of the solar system formed 4.6 billion years ago. Since 1992 more than 1000 Kuiper Belt objects (KBOs) have been detected, mostly outside Neptune's orbit. Three classes of objects are observed: the Plutinos are, like Pluto, in resonant orbit with Neptune, the classical objects have moderately inclined and eccentric orbits, and the scattered disk objects, like the recently discovered 2003 UB_{313}, have large eccentricities and large inclinations. This structure is explained by perturbations by the planets and in particular by resonances with Neptune (Levison & Morbidelli 2003). However, the distance of the belt currently limits the direct detection of KBOs to those with sizes greater than a few tens of kilometers and closer than 100 AU.

Several facts lead to the idea that the known KBOs (>10 km diameter) represent only a small fraction of the Kuiper Belt population. Triton's crater distribution suggests that small impactors (kilometer and subkilometer) have recently riddled this moon (Stern & McKinnon 2000), and so the Kuiper Belt must contain many such bodies. Various collisional simulations reported (Farinella et al. 2000) argue in favor of a significant population of small KBOs. The near-Earth asteroids (NEAs; Rabinowitz et al. 2000) exhibit an almost continuous size distribution from kilometer- to 5 m scale objects. Extrapolating the size distribution of the known KBOs down to objects of 1 km radius leads to 10^{11} KBOs with a total mass of only $\sim 0.1\ M_{\bullet}$ (Gladman et al. 2001). In contrast, a simple extrapolation of the surface mass density of the solar system outside 35 AU yields several Earth masses. Moreover, KBO accretion models require an initial Kuiper Belt 100 times more massive than the currently observed belt and predict that smaller objects of the primitive Kuiper Belt could have been collisionally depleted over the age of the solar system (Malhotra et al. 2000). The outer limit of the belt is also unknown, but beyond 48 AU there does appear to be a sharp decline in the number of objects exceeding 40 km (Allen et al. 2002).

Stellar occultations are a common technique used to study unseen bodies in the solar system, planetary atmospheres, and rings (Sicardy et al. 1991; Millis et al. 1987). The method consists of recording the luminous flux of a star with a fast photometer or a rapid CCD camera. A dip in the stellar light is detected when an occulting object passes between the observer and the star. This method is able to detect small objects inaccessible to direct observation. For example, a star with 1 μas of angular size has a projected size comparable to a 30 m object at 40 AU. Detailed computations (Roques et al. 1987; Roques & Moncuquet 2000), which include diffraction effects, have shown the potential of occultation to detect small objects orbiting in the outer solar system, and in particular beyond the orbit of Neptune. The use of occultations to understand the KBO population has already been suggested in Bailey (1976), Brown & Websters (1997), and Cooray & Farmer (2003), and the Taiwan-American Occultation Survey (Chen 2002) experiment will automatically monitor thousands of stars to search for occultations by intervening KBOs.

2. PRINCIPLE OF THE OCCULTATION TECHNIQUE

The principle of stellar occultation is to record the stellar flux during the transit of an occulting object. Occultation by a KBO is a rapid phenomenon involving Fresnel diffraction. The detection of KBOs by occultation depends on various parameters.

The direction of observation modifies the transverse velocity v of the KBO with respect to the star: $v = v_{\rm E}[\cos(\omega) - R^{-1/2}]$, where $v_{\rm E}$ is the Earth's velocity, ω is the angle from opposition to

[1] Laboratoire d'Etudes Spatiales et d'Instrumentation en Astrophysique, Observatoire de Paris, F-92195 Meudon Principal Cedex, France; francoise.roques@obspm.fr.
[2] Corresponding author.
[3] Department of Physics and Astronomy, University of Sheffield, Sheffield S10 2TN, UK.
[4] Department of Physics, University of Warwick, Coventry CV4 7AL, UK.
[5] National Research Council of Canada, Victoria, BC V9E 2E9, Canada.
[6] Department of Physics and Astronomy, McMaster University, Hamilton, ON L8S 4M1, Canada.
[7] Astronomical Observatory of Kharkiv National University, 61022 Kharkiv, Ukraine.
[8] School of Mathematics and Physics, Queens University Belfast, Belfast BT7 1NN, Northern Ireland, UK.
[9] Observatoire de Besançon, BP 1615, 25010 Besançon Cedex, France.
[10] Grupo de Astrofisicada, Universidade de Coimbra and Observatório de Coimbra, Largo D. Dinis, 3001-454 Coimbra, Portugal.
[11] Istituto Nazionale di Astrofisica, Osservatorio Astrofisico di Arcetri, Largo Enrico Fermi 5, I-50125 Florence, Italy.

TABLE 1
Characteristics of the Occulted Stars

Field	Star	V (mag)	$B-V$	Apparent Radius at 40 AU (m)	Ecliptic Longitude (deg)	Ecliptic Latitude (deg)
Field 1	TYC 281-906	12.10	−0.28	<100	183.5	+2.9
	TYC 281-864	12.15	−0.16	<250	183.5	+2.9
Field 2	TYC 6172-1103	11.81	−0.04	<270	227.0	−0.4
	TYC 6172-1154	12.70	−0.27	<90	227.0	−0.4
Field 3	TYC 6821-1317	12.25	−0.41	<100	254.8	−7.1
	TYC 6821 1425	12.40	−0.32	<100	254.8	−7.1

Notes.—The apparent radius is deduced from the visual magnitude and the spectral class ($B-V$). This is a maximum value since the reddening has not been taken into account.

the line of sight, and R is the radius of the KBO's orbit in AU. The probability of occultation is proportional to v, but the occultation's duration is inversely proportional to this velocity. At opposition, the velocity and the occultation rate are maximum, but the occultation duration is minimum. At quadrature, defined by $\cos(\omega) = R^{-1/2}$, the velocity of the KBO is minimum.

The angular size of the star is a critical parameter because the occultation profile is smoothed over the stellar disk. A stellar radius of 1 mas corresponds to a projected radius at 40 AU of 30 km. Occultation of such stars by a subkilometer KBO does not generate a detectable decrease of the stellar flux. Consequently, the search for small objects needs carefully chosen target stars. They must have a small angular diameter but be bright enough to give a good signal-to-noise (S/N) ratio. Blue stars are the best candidates, because for a given magnitude they have the smallest angular diameter.

The light curve noise constrains the detection of the occultation dip. The S/N ratio is limited by the transparency of the sky (clouds). Scintillation also reduces the S/N ratio for stars brighter than $m_V \approx 12$. However, under good observing conditions with a large telescope, photon noise is the main source of noise in the light curve. In that case, the S/N ratio is proportional to the radius of the telescope. Using synthetic light curves, the depth of the events is compared with the rms fluctuations of light curves for variable telescope sizes. Depending on what one believes about the size distribution of the KBO population, the estimated number of events is 2.5–6 times smaller on a 1 m telescope than on an 8 m telescope (F. Roques et al. 2006, in preparation).

Diffraction must be taken into account for objects on the order of or smaller than F, the Fresnel scale, which is the typical scale of the diffraction pattern: $F = (\lambda R/2)^{1/2}$, where λ is the wavelength and R is the distance to the KBO. The scale $F \approx 1.2$ km for a KBO at 40 AU observed at 0.48 μm. Diffraction reduces the depth of the occultation dip but extends the size of the diffraction shadow and hence the duration of the occultation event. A complete analysis of occultations by KBOs and the modeling of synthetic profiles is given in Roques & Moncuquet (2000).

3. OBSERVATIONS AND DATA REDUCTION

3.1. *Observations*

We conducted a survey for serendipitous occultations in 2004 April using the high-speed triple-beam imaging photometer ULTRACAM (Dhillon & Marsh 2001; Beard et al. 2002), mounted at the Cassegrain focus of the 4.2 m William Herschel Telescope on La Palma. The plate scale on ULTRACAM's three CCD detectors is $0\farcs3$ pixel^{-1}, imaging a field of $\sim 5'$. The stars were monitored using 0.021 s exposures with 0.0007 s of dead time between exposures. We observed three fields on the ecliptic, each containing two main-sequence O stars of approximately equal brightness, selected from the Tycho catalogue (Hog et al. 2000; Table 1). The stars were chosen to ensure a small angular diameter, which is a prerequisite to obtain diffraction fringes. A total of $\sim$1.9 million frames were obtained on the nights of 2004 April 29 and May 2, simultaneously in the g' (0.48 μm) and i' (0.77 μm) Sloan Digital Sky Survey filters (Fukugita et al. 1996).

3.2. *Data Reduction*

Data reduction was carried out using the ULTRACAM pipeline data reduction software. After debiasing and flat-fielding the images, source fluxes were extracted by summing the counts in a circular aperture centered on each target star and subtracting a corresponding sky value determined from the (clipped) mean level in an annulus surrounding the star. To test the robustness of our flux measurement against signal artifacts, we measured stellar fluxes using both fixed apertures (of radii 8, 10, and 12 pixels) and variable apertures (where the radii were determined from fits to the stellar profiles in each frame). The S/N ratio per image varies with the star and the filter used and ranges between 35 and 72 after background subtraction.

4. DATA ANALYSIS

4.1. *Duration of an Event*

The duration of an event is the ratio between the size of the diffraction shadow and the velocity of the occulter in the sky plane. With the assumption of a circular orbit around the Sun, the velocity of the object in the sky plane depends on ω, the angle between the occulter and the antisolar direction. In our observations, $\omega = 36^\circ, 7^\circ$, and 35° for fields 1, 2, and 3, respectively, and $D_{\rm AU}$ is the distance of the occulter from the Sun in AU.

The diameter of the diffraction shadow of a small object is 3 times the Fresnel scale when the star is small with respect to the latter (see F. Roques et al. 2006, in preparation). This leads to diffraction patterns lasting between 0.08 and 0.4 s for orbits of occulters between 4 and 200 AU in the given geometry of our observations.

To detect such events in our time series we computed the standard deviation of the stellar flux and accepted as detections variations larger than 5 σ. High-frequency fluctuations, due to cosmic rays, clouds, and electronic problems, have a clear signature and were eliminated via visual examination of the time series. We also inserted simulated fluctuations created by a synthetic 200 m object at 40 AU into the time series. This synthetic event was clearly detected. We found three events in the 604 minutes of data (Fig. 1, *top panels*).

We have run several checks to assess the validity of our detections. First, detected events should not be seen in the comparison

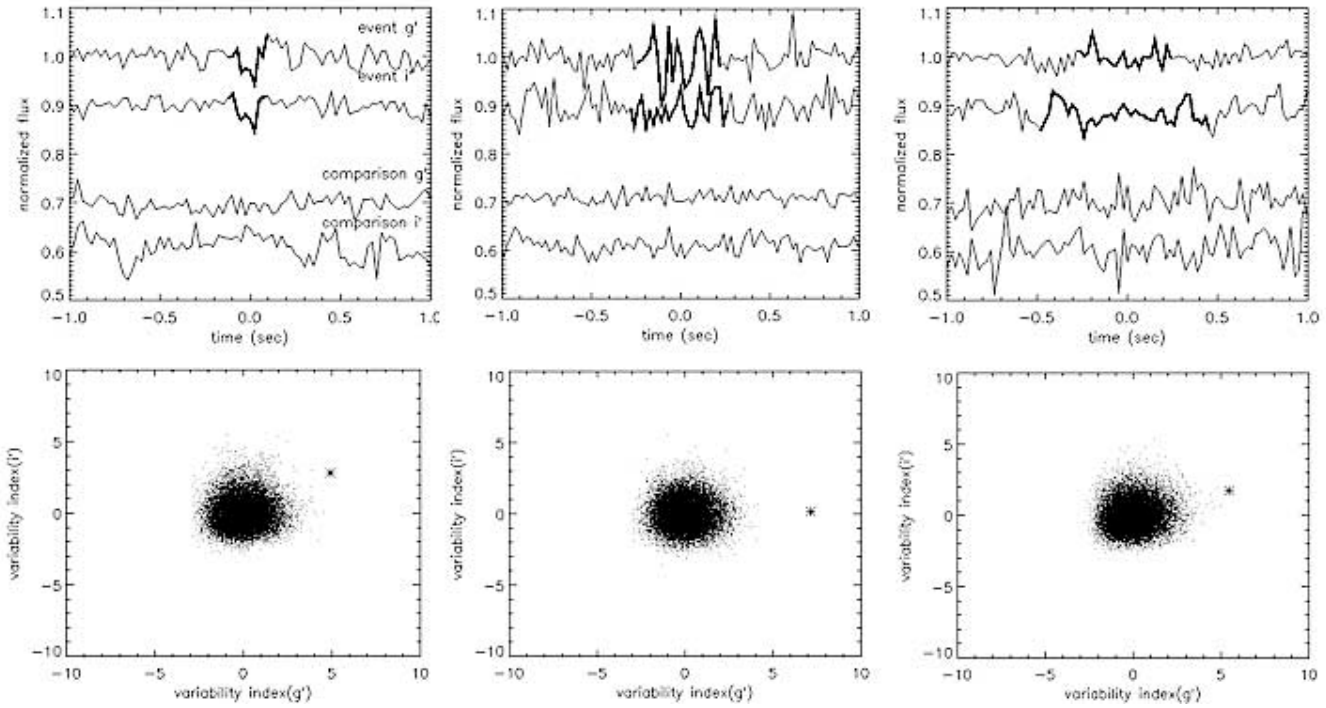

FIG. 1.—Three detected events. *Top panels:* Light curves in the g' and i' bands for the event (*upper curves*) and the comparison star (*lower curves*), respectively. *Bottom panels:* VI of the three events for interval duration of six points (event 1) and 16 points (events 2 and 3). The coordinates of VI(int) are the standard deviation of the normalized stellar flux in the g' and i' channels, relative to the mean standard deviation of the data and expressed in units of standard deviation; sig is the standard deviation for the interval int, and meansig is the mean standard deviation of the data set, where VI(int) = [sig(int) − meansig]/stddev(sig). The events came out clearly above the VI cloud of the data.

star (Fig. 1). We generated false data by randomizing the time series to check that false events due to uncorrelated noise are not selected. We have also checked that the detected events were not due to a star's position (e.g., due to autoguiding errors) or to sky glitches (e.g., cosmic rays or car headlights). As a further test to confirm that our potential events were not actually "routine" flux fluctuation from ordinary scintillation, we analyzed 19 hr of similar photometric data from Neptune and Uranus occultation observations obtained for different purposes (Sicardy et al. 1991). The conditions of observation were similar, but, with a projected radius >10 km at 40 AU, these stars should not have shown diffraction occultation events. Using the same procedure as described above, we did not detect any event that mimics diffraction in this "null" set.

To assess that our three detections are not due to noise, we further defined a vectorial variability index (VI) for data intervals. For a given interval, one can define VI(int), whose coordinates are the standard deviation of the normalized stellar flux in the g' and i' channels. This standard deviation is computed with respect to the mean standard deviation of the data and is expressed in units of standard deviation: if sig = stddev(int) for the standard deviation for the interval int and meansig is the mean standard deviation of the data (for the whole night), then VI(int) = [sig(int) − meansig]/stddev (sig).

For purely random data, the VI in a two-dimensional plot appears as an isotropic cloud centered around the mean (0, 0). Data are Gaussian-distributed and thus concentrated around the mean. In consequence any deviant point should be a clear detection of a nonrandom event.

Figure 1 (*bottom panels*) shows the VI for the three detected events. Any deviant point is the detection of a nonrandom event. The three events are outside the noise clusters. For the noise, the

TABLE 2
SIZE AND DISTANCE OF THE DETECTED OBJECTS

Object (1)	Object Radius (m) (2)	Orbit Radius ($e = 0$) (AU) (3)	Semimajor Axis (AU) (4)	Occulted Star (5)
1.....	110	15 ± 5	9–19[a]	6821-1317
2.....	320	140 ± 17	115–150[b]	6172-1154
3.....	300	210 ± 21	182–225[b]	6172-1103

NOTES.—The detected events are compared with synthetic diffraction profiles and are fitted with two parameters: the distance of the object from the Sun and the object's radius. The object orbit is circular, and the impact parameter (minimum distance from the center of the shadow to the star path) is set to zero. The error on the orbit radius is computed from the event duration (see the text).

[a] $e = 0.2$.

[b] $e = 0.4$.

modulus of VI is $\leq$4.5, and the moduli of VI for the three events are, respectively, 5.6, 7.2, and 5.3.

Having shown that the events are neither related to the observation's conditions nor to the Earth's atmosphere, we compare them to diffraction profiles of interplanetary objects. The synthetic profiles depend on two parameters: the object's radius and its distance from the Sun. The synthetic profile is computed assuming a circular orbit and zero-impact parameter. The parameters of the synthetic profiles given in Table 2 (cols. [1] and [2]) are the best fit for the three events. The hypothesis of a zero-impact parameter corresponds to a minimum distance. Noncircular orbits transform the orbit parameter into a range of semimajor values (Table 2, col. [4]). Note that the duration of event 1 is larger in i' data (0.77 μm) than in g' data (0.48 μm) due to diffraction. The i' profiles of events 2 and 3 are too noisy to check this relation.

Diffraction enables one to estimate directly the distance of an occulter from a single observation. For objects smaller than half the Fresnel scale, the diameter of the diffracting shadow does not depend on the object's size and is proportional to the Fresnel scale. On the other hand, the duration of an occultation is directly related to the distance of the object from the Sun (Kepler's Third Law). Assuming a circular orbit and zero-impact parameter, the profile provides an estimate of the distance of the occulter. The relative error of this estimate can be computed from the uncertainty in the duration.

There are two mathematical solutions for a given occultation duration. The nearer solutions would give orbits between 1 and 1.6 AU for the three objects. The corresponding sizes of the objects would be smaller, by a factor equal to the square root of the ratio of the distance (e.g., 25 m at 1 AU for objects of 300 m at 140 AU). With these nearby solutions, the objects would be NEAs. The number of detected objects would imply billions of NEAs in this size range, which is not compatible with the known size distribution.

Another method, developed independently by S. B. and J. J. K., was used to search for the events (Bickerton et al. 2004). Candidate occultation events were identified by convolving the observed photometric time series with synthetic diffraction patterns. The three diffraction events were also detected by this method.

5. RESULTS AND DISCUSSION

Three heretofore undetectable subkilometer-size objects were detected. (1) Object 1 corresponds to an orbit of 15 AU. However, its orbit could also be moderately eccentric with semimajor axis equal to that of Saturn's or Uranus's orbit. (2) No object was detected in the classical Kuiper Belt between 30 and 60 AU, where 100 m objects would be detectable. Our 10 hr of observation scanned $10^{-8}\,R_{\rm AU}^{-1.5}$ deg^2 of the sky plane at the distance R from the Sun. This nondetection, combined with previous observations (Roques et al. 2003), constrains the number of objects in this region (Fig. 2)

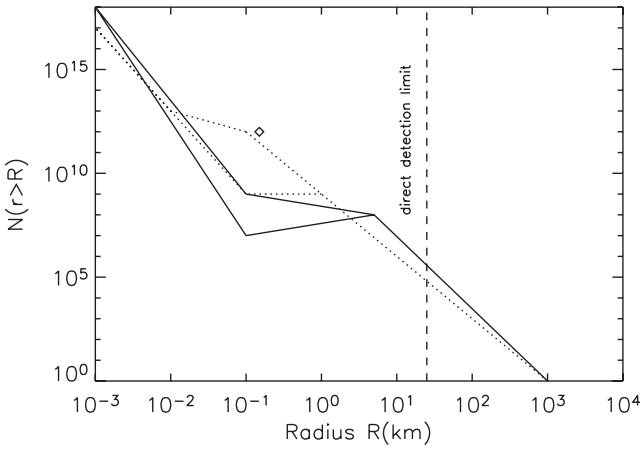

FIG. 2.—Cumulative size distribution of the Kuiper Belt. The dashed line is the limit from the evolutionary model (Kenyon & Bromley 2004), taking into account stirring by Neptune (*solid lines*) or not (*dotted lines*). In each case, the two lines correspond to weak (*lower*) or strong (*upper*) KBOs. The diamond is the constraint from the nondetection of objects in our observation when 200 m objects are detectable.

and leads to a maximum mass of 0.5 $M_\bullet$. This constraint is independent of albedo. (3) Two 300 m radius objects were found beyond 100 AU. These objects are in the ecliptic plane. They may be small members of a cold, thin, and extended disk of the Kuiper Belt. This implies a large population of small objects in the outer (50–150 AU) solar disk that could represent a large fraction of Earth's mass. Further observations will allow us to constrain the mass and spatial distribution of this disk. The limit of direct detections (Bernstein et al. 2004) could be due to a decrease in the KBO maximum size beyond 50 AU. Our observations provide the first detections in this region of the solar system, and further observations are needed to discriminate between the various hypotheses. Stellar occultation is the only detection method available to identify dark matter in the outer region of the disk, which is not perturbed by the planetary resonances as is the inner part, which is explored by direct observation. Future occultation observations will clarify the structure, mass, and size of this primitive part of the solar disk.

We thank the Programme National de Planétologie for financial support of this research and the Panel for the Allocation of Telescope Time for consistent allocation of telescope time. N. P. acknowledges funding from Fundação do Ministério de Ciência e Tecnologia, Portugal (grant SFRH/BD/1094/2000).

REFERENCES

Allen, R. L., Bernstein, G. M., & Malhotra, R. 2000, AJ, 124, 2949
Bailey, M. E. 1976, Nature, 259, 290
Beard, S. M., et al. 2002, Proc. SPIE, 4848, 218
Bernstein, G. M., Trilling, D. E., Allen, R. L., Brown, M. E., Holman, M., & Malhotra, R. 2004, AJ, 128, 1364
Bickerton, S. J., Kavelaars, J. J., & Welch, D. L. 2004, BAAS, 36, 1103
Brown, M. J. I., & Webster, R. L. 1997, MNRAS, 289, 783
Chen, W. P. 2002, Highlights Astron., 12, 245
Cooray, A., & Farmer, A. J. 2003, ApJ, 587, L125
Dhillon, V. S., & Marsh, T. 2001, NewA Rev., 45, 91
Farinella, P., Davis, D. R., & Stern, S. A. 2000, in Protostars and Planets IV, ed. V. Mannings, A. P. Boss, & S. S. Russell (Tucson: Univ. Arizona Press), 1255
Fukugita, M., et al. 1996, AJ, 111, 1748
Gladman, B. J., Kavelaars, J. J., Petit, J., Morbidelli, A., Holman, M. J., & Loredo, T. 2001, AJ, 122, 1051
Hog, E., et al. 2000, A&A, 355, L27
Kenyon, S. J., & Bromley, B. C. 2004, AJ, 128, 1916
Levison, H. F., & Morbidelli, A. 2003, Nature, 426, 419
Malhotra, R., Duncan, M., & Levison, H. 2000, in Protostars and Planets IV, ed. V. Mannings, A. P. Boss, & S. S. Russell (Tucson: Univ. Arizona Press), 1231
Millis, R. L., et al. 1987, Icarus, 72, 507
Rabinowitz, D., Helin, E., Lawrence, K., & Pravdo, S. 2000, Nature, 403, 165
Roques, F., & Moncuquet, M. 2000, Icarus, 147, 530
Roques, F., Moncuquet, M., Lavillonière, N., Auvergne, M., Chevreton, M., Colas, F., & Lecacheux, J. 2003, ApJ, 594, L63
Roques, F., Moncuquet, M., & Sicardy, B. 1987, AJ, 93, 1549
Sicardy, B., Roques, F., & Brahic, A. 1991, Icarus, 89, 220
Stern, A., & McKinnon, W. B. 2000, AJ, 119, 945